Applied Catalysis B: Environmental 176–177 (2015) 586–593

Contents lists available at ScienceDirect

Applied Catalysis B: Environmental

journal homepage: www.elsevier.com/locate/apcatb

# Template-assisted in-situ synthesis of porous AgBr/Ag composite microspheres as highly efficient visible-light photocatalyst

Shiyun Lou, Xianbin Jia, Yongqiang Wang*, Shaomin Zhou**

*Key Laboratory for Special Functional Materials of the Ministry of Education, Henan University, Kaifeng 475004, PR China*

ARTICLE INFO

*Article history:*
Received 2 February 2015
Received in revised form 8 April 2015
Accepted 10 April 2015
Available online 17 April 2015

*Keywords:*
CuBr template
AgBr/Ag composite microspheres
Visible-light
Photocatalyst

ABSTRACT

A novel one step template-assisted in-situ synthetic route was established to synthesize porous AgBr/Ag composite microsphere. Herein, CuBr microsphere was selected as a chemical template to generate porous AgBr/Ag composite microsphere via one step in-situ reaction, where, CuBr not only provided $Br^-$ ion to generate AgBr but also released $Cu^+$ ion to reduce $Ag^+$ ion into elemental Ag. The experimental results revealed that the AgBr/Ag composite microsphere could be obtained easily and quickly with the established in-situ synthetic route, while the composition (the ratio of AgBr to Ag) of the final products could be tuned through changing the ratio of CuBr template to $Ag^+$ ion in the precursor solution. Besides, the in-situ formation procedure of porous AgBr/Ag composite microsphere was investigated and found that the template-assisted in-situ synthesis of porous AgBr/Ag composite microsphere was dominated by a kind of synergistic in-situ reaction mechanism involving the ion-exchange reaction between CuBr microsphere and $Ag^+$ as well as follow-up in-situ reduction reaction of $Ag^+$ ion by $Cu^+$ ion released from the CuBr template. The photocatalytic performance of the as-synthesized AgBr/Ag composite microspheres with different compositions were evaluated by monitoring the decolorization of methyl orange (an organic dye; denoted as MO) and the degradation of phenol under visible-light irradiation, and the as-synthesized porous AgBr/Ag composite microsphere with AgBr/Ag ratio of 1:1 was capable of bleaching 94% MO within 20 min while it can decompose 79% of phenol in 180 min, showing excellent visible-light photocatalytic activity.



## 1. Introduction

Photocatalysis, as a green chemistry technology, is becoming a promising approach to solving many serious environmental problems with the utilization of solar energy [1]. During the past decades, lots of semiconductor nanostructures have been widely investigated as photocatalysts for environmental decontamination applications [2]. $TiO_2$, as a typical semiconductor photocatalyst, can utilize no more than 5% of the total solar energy due to the wide band gap (3.0–3.2 eV) [3,4]. To effectively use the visible light that comprises 43% of sunlight, considerable efforts have been devoted to designing photocatalyst for high absorption coefficients in the visible-light region, and thus, the visible-light-driven photocatalysts become an attractive research field for their high utilization efficiency of solar energy [5]. At present, the previous well-studied semiconductors like $TiO_2$ can be further transformed into visible-light-driven photocatalysts through two ways including doping photocatalysts with various transition metals or non-metal atoms and anchoring organic dye molecules on the surfaces of photocatalysts [6]. Although doping wide bandgap photocatalysts could enhance their absorption under visible light, photocatalytic performance still needs to be significantly improved for practical applications. The photocatalysts sensitized by dye molecules exhibited relative high catalytic efficiency, but the stability is problematic in applications such as decomposition of organic pollutants because the dye sensitizers have to bear self degradation. Therefore, new structures or materials are being pursued and developed successively for high efficient visible-light-driven photocatalysts [7].

Recently, noble metal plasmonic nanoparticles (such as Au and Ag) were used to decorate photocatalysts for their resistive against degradation and high absorption coefficients in a broad UV–vis-NIR spectral range due to their strong surface plasmon resonance (SPR) [8,9]. Previous studies indicated that silver halides, especially decorated with silver nanoparticles, possessed excellent photocatalytic activity in the visible-light region [10]. Large amount of experimental results show that the silver halides/silver compos-

* Corresponding author. Tel.: +86 371 23881358; fax: +86 371 23881358.
** Corresponding author.
*E-mail addresses:* wangyq@henu.edu.cn (Y. Wang), smzhou@henu.edu.cn (S. Zhou).

http://dx.doi.org/10.1016/j.apcatb.2015.04.027
0926-3373/

ite materials exhibit high absorption coefficients in a broad UV–vis spectral range due to the strong SPR of silver nanoparticles [11–25]. Furthermore, these silver nanoparticles could trap electrons during the separation of photo-generated electron–hole pairs and enhance photocatalytic efficiency. Meanwhile the stability of the silver halides based composite photocatalysts were also enhanced greatly [26–28].

Until now, various methods have been developed to synthesize silver halides/silver micro/nanostructures including microsphere, nanowire or nanotube, cage and so on [29–34]. Among the various methods, template methods have attracted the attention of many researchers because the pre-existing guide with desired nanoscale features could direct the formation of nanomaterials into forms that are otherwise difficult to obtain [35]. For example, Choi et al. have synthesized Ag derivatives (AgX@Ag (X = Cl and Br), or Ag nano/microtubes) using the AgCl nanowires as templates [30]. Wang et al. reported the synthesis of AgBr/Ag composite particles through ion-exchange of $Ag_2MoO_4$ template with HBr [31]. Tang et al. and Xiao et al. fabricated the AgCl/Ag and Ag@AgBr cubic cages using a water-soluble sacrificial salt-crystal-template process, respectively [32,33]. Although the previous reported template methods could realize the synthesis silver halides/silver composites, an additional reducing step with regard to chemical reduction, or light-induced reduction has been used to generate metallic Ag species in the produced products. In addition, the content of Ag is hard to control during synthesis. Thus, a lower cost and facile synthetic method for the preparation of highly effective and reproducible photocatalyst is still in great demand.

Herein, monodisperse CuBr microsphere was employed as template to synthesize AgBr/Ag composite microsphere in one step, in which CuBr microsphere could provide both $Br^-$ ion and $Cu^+$ ion to react with $Ag^+$ ion and generated AgBr and elemental Ag, respectively. The composition (the ratio of AgBr to Ag) of the AgBr/Ag composite microsphere could be controlled by adjusting the ratio of $AgNO_3$ to CuBr template. According to serial experimental results, a kind of in-situ synergistic reaction mechanism was proposed that the ion-exchange reaction between CuBr and $Ag^+$ ion proceeded firstly to generate AgBr frame and then the released $Cu^+$ ion reacted with $Ag^+$ ion nearby to form Ag nanoparticle in-situ. Furthermore, the photocatalytic performance of porous AgBr/Ag composite microsphere with different composition (the ratio of AgBr to Ag) was investigated through the decolorization of MO and the degradation of phenol under visible-light irradiation in detail.

## 2. Experimental

### 2.1. Materials

Copper(II) bromide ($CuBr_2$), silver nitrate ($AgNO_3$), L-ascorbic acid, polyvinylpyrrolidone (PVP K30), and ethanol were purchased from Sinopharm Chemical Reagent Co., Ltd., all chemicals were of analytical grade and used without further treatments. Water used throughout all these experiments was purified with a Millipore system.

### 2.2. Synthesis of the photocatalyst

Uniform CuBr microspheres were synthesized according to earlier literature with some modifications [36]. In a typical procedure, an aqueous solution was first prepared by mixing 100 mL of water, 10 mL of PVP solution (10 wt%), and 1.0 mL of $CuBr_2$ solution (0.5 M). Then 5.0 mL of ascorbic acid solution (0.5 M) was added to the solution, and the mixture became turbid shortly, indicating the formation of CuBr particles. The mixture was stirred for 5 min and the obtained products were washed with ethanol four times and then dried in vacuum at 60 °C for 6 h.

For synthesizing AgBr/Ag composite microspheres, the obtained CuBr microspheres were dispersed in 80 mL of ethanol. Meanwhile, a certain amount of $AgNO_3$ was dispersed in 20 mL of ethanol. The above two solutions were mixed and vigorously stirred with magnetic stirrer for one minute. After the reaction was over, the precipitate was harvested by centrifugation, and washed with deionized water and ethanol repeatedly. Finally, the obtained products were dried at 60 °C for 6 h in a vacuum oven.

For comparison, the visible-light-driven photocatalyst nitrogen-doped $TiO_2$ (denoted as N-$TiO_2$) was prepared by calcination of P25-$TiO_2$ at 600 °C for 4 h under $NH_3$ atmosphere.

### 2.3. Characterization

Phase identification and structure analysis of the products were analyzed by a Bruker D8 Advance X-ray diffractometer with Cu Kα radiation with diffraction angle ($2\theta$) range of 20–80°. The morphologies of the prepared AgBr/Ag composite microspheres were studied by field emission scanning electron microscopy (FESEM, FEI, Nova Nano SEM 450) and transmission electron microscopy (TEM, JEOL-2010, 200 kV). Ultraviolet–visible (UV–vis) absorption spectra were collected with a UV–vis spectrophotometer (Cary 5000 UV–vis-NIR spectrophotometer). X-ray photoelectron spectroscopy (XPS) was performed on an AXIS ULTRA X-ray photoelectron spectrometer using 300 W Al *Ka* radiation. The specific surface areas of the products were measured by using a Quadrasorb SI apparatus (Quantachrome Corporation, USA) and the specific surface areas were estimated in terms of the Brunauer–Emmett–Teller (BET) method.

### 2.4. Photocatalytic activity

Methyl orange (MO) was chosen as the target organic compound in this study to probe the photocatalytic performance of various prepared photocatalysts. In a typical performance, 30 mg of respective photocatalysts were dispersed in a 30 mL of aqueous solution of methyl orange (MO) dye (10 mg $L^{-1}$). The dispersion was kept in the dark for 30 min for dark adsorption experiment, after which the photo decolorization was carried out. The light source was a 500 W Xenon lamp installed in a laboratory lamp housing system. Before entering the reactor, the light passed through a UV cut-off filter (>400 nm). Aliquots of the suspension (5.0 mL) at respective irradiation time intervals were collected, and centrifuged to remove the photocatalysts. The samples were analyzed quantitatively for the absorption peak at 464 nm generated under UV–vis absorption spectrometer (Shanghai Instrument Analysis Instrument Co., Ltd.). The recycling tests are performed according to the above procedure after centrifugation.

In addition, phenol was selected as a target organic pollutant to probe the visible-light-driven activity of various prepared photocatalysts because it is a colorless, non-volatile and common contaminant present in industrial wastewaters and the mechanism of phenol decomposition is also well established both under UV and visible-light irradiation [37–42]. In a typical performance, 50 mg of respective photocatalysts were dispersed in a 40 mL of aqueous solution of phenol (10 mg $L^{-1}$). The experimental condition was the same as that of the bleaching of MO. In the process of photocatalysis, aliquots of the suspension (5.0 mL) at respective irradiation time intervals were collected, and centrifuged to remove the photocatalysts and analyzed using a high-performance liquid chromatography (HPLC; Agilent 1100) system equipped with a diode array ultraviolet detector. The HPLC system included a C18-reverse phase column with a mobile phase of acetonitrile (70%)-water (29.5%)-phosphoric acid (0.5%); a flow rate of 0.4 mL/min.

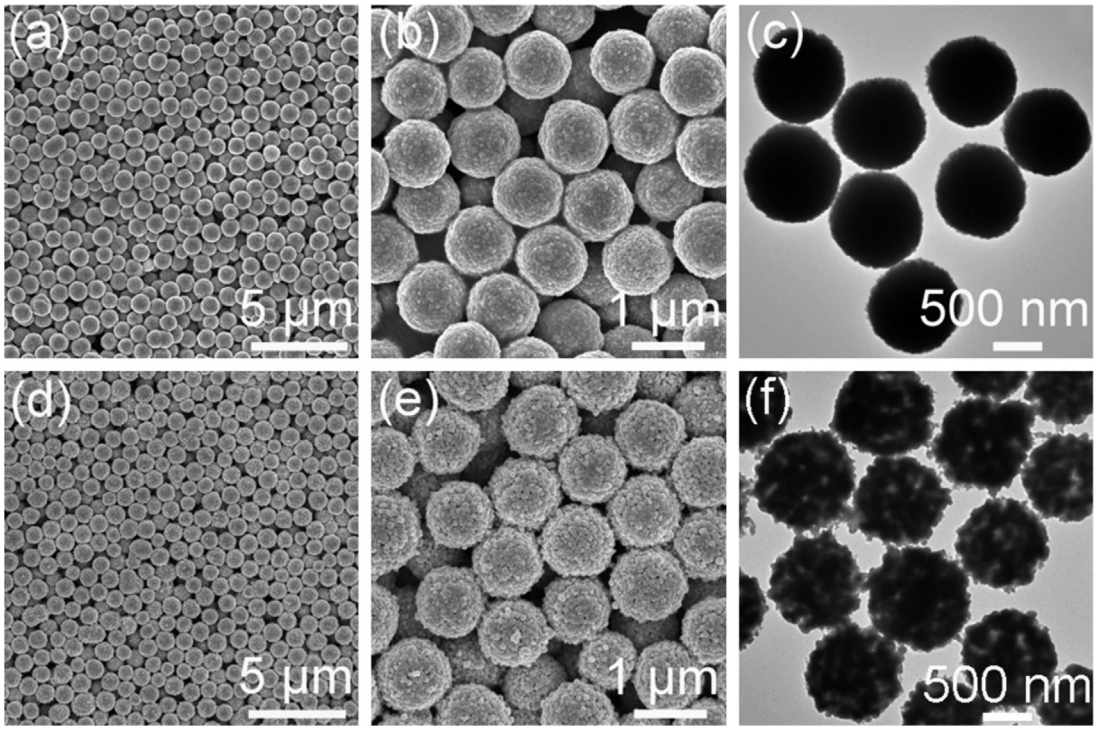


**Fig. 1.** Typical SEM and TEM images of (a–c) CuBr microspheres and (d–f) AgBr/Ag microspheres.

Quantification of phenol and the degradation products was performed using a photodiode-array detector at 269 nm.

## 3. Results and discussion

### 3.1. Characterization of AgBr/Ag composite microspheres

As seen in Fig. 1a, uniform CuBr microspheres as chemical template in our experiment could be synthesized in a large scale through a simple room-temperature reaction. The CuBr microspheres composed of nanoparticles in Fig. 1b, are uniform with an average diameter of about 900 nm, and these microspheres exhibit relatively rough surface and a solid internal structure from the TEM image in Fig. 1c. The XRD pattern revealed these microspheres were CuBr with cubic structure from all the diffraction peaks (JCPDS No. 06-0292) in Fig. S1a. After reaction, the original XRD peaks of CuBr microspheres disappeared and new peaks were found and could be indexed to face-centered cubic structure Ag (JCPDS No. 87-0717) and AgBr crystal structure (JCPDS No. 79-0149) in Fig. S1b, indicating the formation of AgBr/Ag composites. Meanwhile no peaks of CuBr microspheres were detected, indicating the CuBr templates were transformed into AgBr/Ag composites. Additionally, the energy dispersion X-ray spectrum (EDS) of the AgBr/Ag microspheres further proved that the product consisted of only Ag and Br element (Fig. S2b), and no Cu element was detected after the reaction, revealing the generation of AgBr/Ag composites as well. The morphology of the final AgBr/Ag product was observed by SEM image in Fig. 1d, which still kept well-defined and uniform spherical morphology with similar size with the original CuBr microspheres, which indicated the AgBr/Ag generated in-situ by using CuBr template. Although AgBr/Ag composite microspheres kept the original structure, the surface of microspheres became rough obviously in Fig. 1e and the interior of microsphere became porous, which is different from the original solid CuBr microspheres in Fig. 1c. The above characterizations proved that AgBr/Ag composite microspheres were successfully synthesized by simple using CuBr microspheres as chemical template in one step.

### 3.2. The structural investigation of AgBr/Ag composite microspheres

In our experiment, the CuBr microspheres were employed as chemical template to provide both $Br^-$ and $Cu^+$ sources. Therefore, two reactions according to the below equations took place during the formation process of AgBr/Ag composite microspheres [12,43].

$$CuBr + Ag^+ = AgBr + Cu^+ \quad (1)$$

$$Cu^+ + Ag^+ = Ag + Cu^{2+} \quad (2)$$

Since both $Br^-$ and $Cu^+$ ions could react with $Ag^+$ ions, the investigation of the ratio between CuBr and $Ag^+$ is very important to adjust the ratio of AgBr to Ag in final products. A series of experiments were conducted to explore the influence of the amount of $Ag^+$ ions while other parameters kept the same. The molar ratios of $Ag^+$ ions to $Cu^+$ ions (calculated from the amount of CuBr template) were changed from 0.5:1 to 3:1. Upon the addition of different amount of $AgNO_3$ aqueous solution at room temperature, the reaction proceeded quickly, which could be judged through the color change of initial white solution to brown black quickly in one minute, because of the big difference of solubility products (Ksp) of CuBr ($5.9 \times 10^{-9}$ mol/L) and AgBr ($5.0 \times 10^{-13}$ mol/L) and reducing capability of $Cu^+$ ions according to the above two equations.

In the XRD patterns in Fig. 2, it was surprising to observe that when the moral ratio of CuBr to $AgNO_3$ was 0.5:1, only AgBr was detected from XRD peaks in Fig. 2b, meanwhile the original peaks of CuBr disappeared completely. The XRD peaks of Ag could be found when moral ratio of $AgNO_3$ to CuBr reached to 1:1 in Fig. 2c, which became stronger when the moral ratio increased to 2:1 and 3:1 in Fig. 2d and e. The above serial experiments primarily indicated that the two reactions including ion-exchange reaction between CuBr and $Ag^+$ and reduction between $Cu^+$ and $Ag^+$ did not proceed simultaneously, and ion-exchange reaction between CuBr and $Ag^+$

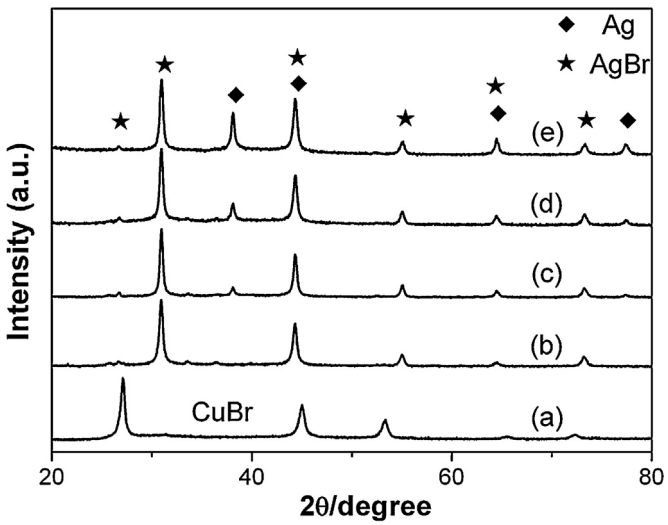


**Fig. 2.** XRD patterns of (a) CuBr template and the products synthesized with different molar ratios of $AgNO_3$ to CuBr: (b) 0.5:1, (c) 1:1, (d) 2:1, and (e) 3:1.

took place obviously faster than the reduction of $Ag^+$ by the released $Cu^+$ ions, since only XRD peaks of AgBr were observed when the molar ratio of $AgNO_3$ to CuBr was 0.5:1. It was worth noting that when the moral ratio of $AgNO_3$ to CuBr was 0.5:1, half of the original CuBr should be remained in the microsphere according to Eq. (1), however, no XRD peaks of CuBr was observed. After a controlled experiment, it was found that CuBr was rather unstable, and could be dissolved in ethanol spontaneously, therefore, no XRD peaks of CuBr were detected even with less $AgNO_3$ in precursor solution.

The morphologies of the above series products were further characterized by SEM. As seen from Fig. 3a–d, all the products synthesized with different molar ratio of $AgNO_3$ to CuBr present uniform spherical structure and similar size. Although their magnified images show that the as-obtained microspheres were all composed of nanoparticles, the pack densities and roughness were clearly different. As seen from Fig. 3e–h, when the amount of $Ag^+$ was lower than 1:1, the nanoparticles were loosely stacked and lots of pores could be clearly seen from the surface of the microspheres in Fig. 3e, however, the pores could be hardly detected when the amount of $Ag^+$ was higher than 1:1, especially at 3:1 in Fig. 3h. The reason was proposed that since ion-exchange reaction between CuBr and $Ag^+$ was proved to take firstly, the porous AgBr microsphere formed before the reduction of $Ag^+$ ion. Besides, the $Ag^+$ ion existing in the AgBr microsphere was reduced to elemental Ag by $Cu^+$ ion, as a result, the pores of AgBr microsphere would be filled and became smaller even disappeared as seen in Fig. 3f–h.

The above products were characterized by EDS and XPS to further investigate their compositions. As shown in Fig. S2, only Ag and Br elements were detected in the energy dispersion X-ray spectrum (EDS) of the AgBr/Ag microspheres from Fig. S3a–d, which revealed that the CuBr template disappeared totally after reaction. Furthermore, the ratios of peak intensity between Ag and Br increased with the molar ratio of $AgNO_3$ to CuBr increased in the reaction, indicating more elemental Ag generated in the final products. The XPS spectra (Fig. S3) of the Ag species of the bare AgBr/Ag display two bands at ca. 373 and 367 eV, which can be attributed to Ag $3d_{3/2}$ and Ag $3d_{5/2}$ binding energies, respectively. These two bands could further be deconvoluted into two groups of peaks at 373.0, 374.5 eV and 367.0, 367.5 eV. Those at 374.5 and 367.5 eV are ascribed to the metallic Ag of AgBr/Ag, and those at 373.0 and 367.0 eV are ascribed to $Ag^+$, respectively [17,18,44,45]. The calculated surface molar ratios of the metallic Ag to $Ag^+$ (namely, the ratios of Ag to AgBr) in AgBr/Ag composite microspheres are calculated to be 1:25, 1:12, 1:8 and 1:6 in Fig. S3, respectively. The ratio values verify again that the elemental Ag increased when more silver precursor was added.

Although the above crystallographic, morphological and elemental analysis could prove the final microspheres consist of AgBr and Ag with different ratio quantitatively, their distribution in the composite microsphere was still unknown and could not be identified from the above characterizations, which is critical to both formation mechanism and photocatalytic performance analysis. From the TEM image of a single microsphere, the AgBr and Ag ingredients were hardly to indentify for their similar contrast from in Fig. 4a. The AgBr/Ag composite microspheres were further characterized through mapping analysis to investigate the Ag and Br distribution. As shown in Fig. 4c–d, by using SEM mapping analysis of the product in Fig. 4b, it can be seen that Ag element was distributed evenly to the same degree as that of Br. It was not surprising if the microsphere was only composed of AgBr, however, the product here was composed of AgBr and Ag. Thus, it can be concluded indirectly that the elemental Ag distributed evenly in the AgBr/Ag composite microspheres, too. If the generated elemental Ag was just or mostly distributed on the surface of the microspheres, the population of color point of Ag element should be higher on the periphery than that of Br element, vice versa. Meanwhile, the fact that the elemental Ag distributed evenly also indirectly revealed that the $Ag^+$ ions were reduced in-situ in the interior of preformed AgBr microspheres.

### 3.3. Formation mechanism of AgBr/Ag composite microspheres

The formation process of the AgBr/Ag porous microspheres was too fast to be sampled by the time-dependent experiments due to the great difference of solubility products (Ksp) of CuBr ($6.27 \times 10^{-9}$ mol/L) and AgBr ($5.35 \times 10^{-13}$ mol/L). However, the reaction mechanism could be proposed based on the above experiment results, as illustrated in Fig. 5. (a) The CuBr microspheres were synthesized by a chemical method at room temperature, which were composed of nanoparticles with lots of gaps in its surface and interior. (b) After the $Ag^+$ ions were added to the solution, AgBr was firstly generated through ion-exchange of CuBr at the surface of template, and more AgBr would be generated subsequently when $Ag^+$ ions diffused into the interior of CuBr template until it was consumed up. Finally, porous AgBr skeleton was formed in-situ. Since, the generated AgBr copied the CuBr template, the diameter of these AgBr/Ag composite microspheres remains unchanged. (c) During the ion-exchange process, lots of $Cu^+$ ions were released

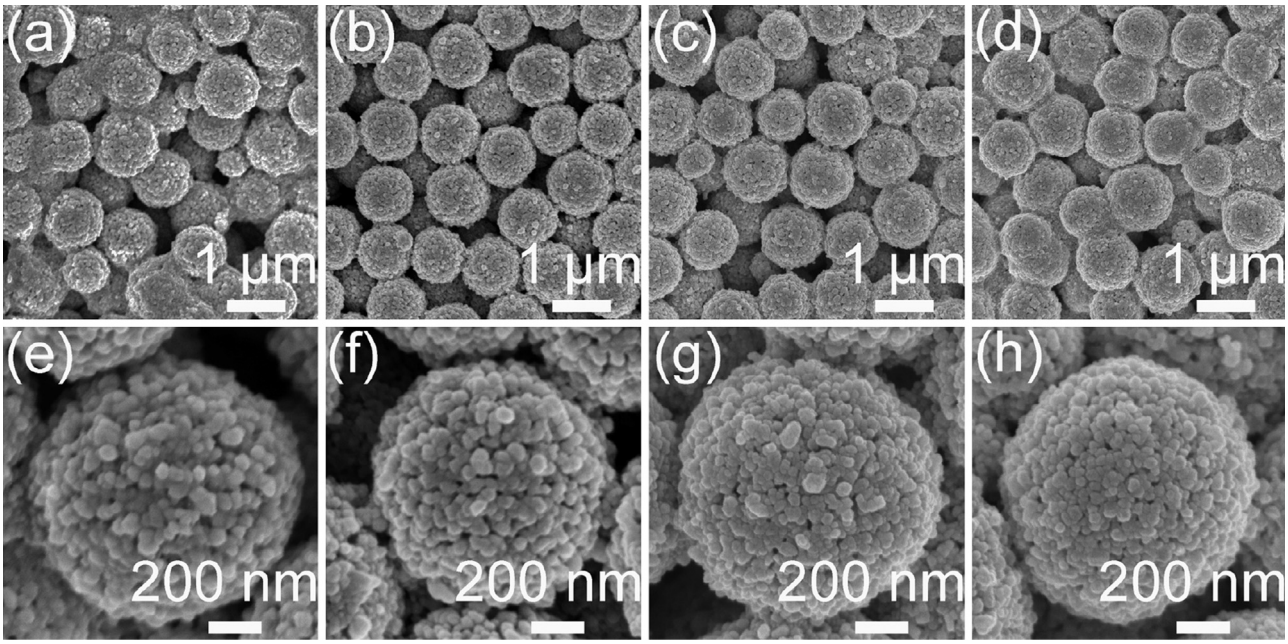


**Fig. 3.** SEM images of the products synthesized with different molar ratios of $AgNO_3$ to CuBr: (a) 0.5:1, (b) 1:1, (c) 2:1, (d) 3:1, and their corresponding magnified images (e–h).

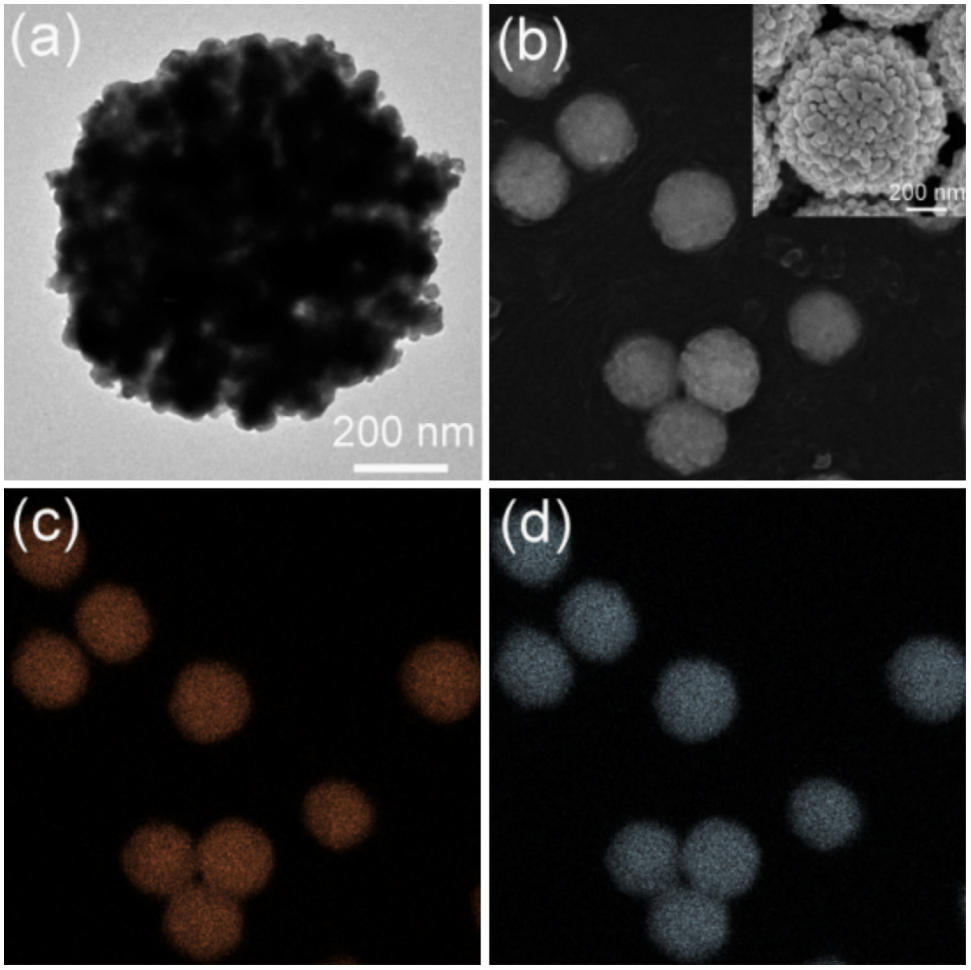


**Fig. 4.** (a) TEM image of a single AgBr/Ag composite microsphere; (b) SEM image of several AgBr/Ag composite microspheres (Inset shows the SEM image of a single microsphere); elemental mapping images of (c) Ag and (d) Br.

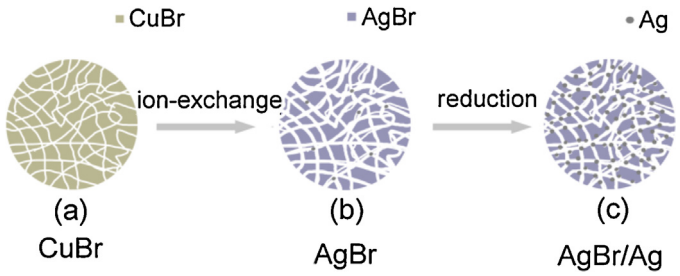


**Fig. 5.** Schematic illustration about the controlled synthesis of AgBr/Ag porous microsphere by a template method.

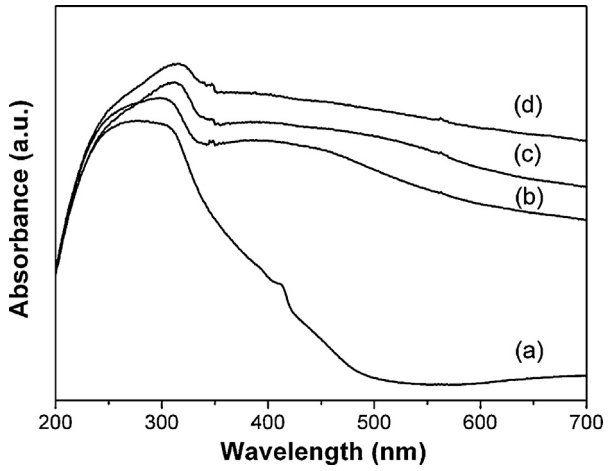


**Fig. 6.** UV–vis absorption spectra of the products synthesized with different ratios of $AgNO_3$ to CuBr: (a) 0.5:1, (b) 1:1, (c) 2:1, and (d) 3:1.

from CuBr template and would reduce the $Ag^+$ ions nearby into Ag nanoparticles, which deposited onto the surface of AgBr skeleton. Since the reaction between $Ag^+$ and $Cu^+$ ions took place later, the Ag content in the final product could be controlled by simple adjusting the amount of $Ag^+$ ions. According to the above proposed formation process, a kind of synergistic reaction mechanism was that the ion-exchange reaction proceeded between CuBr microspheres and $Ag^+$ followed by in-situ $Ag^+$ reduction reaction. This kind of special synergistic formation mechanism provided a simple way to synthesize AgBr/Ag porous microspheres, meanwhile the ratio of AgBr to Ag in final products could be controlled easily by simple adjusting the ratios of $AgNO_3$ to CuBr in precursor solution.

### 3.4. Optical properties and photocatalytic performance of AgBr/Ag porous microspheres

The absorption spectra of AgBr/Ag catalysts with different ratios of $AgNO_3$ to CuBr were analyzed by UV–vis absorption spectra in the wavelength range of 200–700 nm shown in Fig. 6. It can be seen that the AgBr can absorb solar energy with wavelengths shorter than 490 nm in Fig. 6a, which agreed with the results reported previously [27]. When decorated with Ag nanoparticles, the samples exhibit enhanced absorption in the visible-light region in comparison with AgBr microspheres. The strong and broad absorption larger than 430 nm should result from the strong SPR of Ag nanoparticles. Moreover, this band shifted to high wavelength and became broadened when the ratio of $AgNO_3$ to CuBr increased. It is known that the SPR frequency depends closely on the size and shape of particles, inter-particle spacing, and local dielectric environment [9]. The observed change in the SPR absorption band could be ascribed to the increased proportion of $AgNO_3$ and CuBr which is in agreement with XPS results. All of the AgBr/Ag composites show clearly an optical response in the visible region. They all have strong absorption in the UV–vis-light region from 200 to 700 nm, implying that these samples have good visible-light photocatalytic activity.

The photocatalytic activities of the as-prepared AgBr/Ag samples were investigated by the decolorization of methyl orange (MO) under visible light. For comparison, P25-$TiO_2$ was used and its relative information was provided in Fig. S4. As seen in Fig. 7, the AgBr/Ag composite microspheres showed superior photocatalytic activity; and the AgBr/Ag ($AgNO_3$:CuBr = 1:1) composite microspheres can nearly completely decolorize 10 mg $L^{-1}$ MO within 20 min of visible-light irradiation while the P25-$TiO_2$ can only decompose 15% of MO during the same interval. The photolysis experiment without photocatalyst showed any observable decrease in MO concentration with time, demonstrating that photocatalysis was indeed the cause for the decolorization of MO.

As plotted in Fig. 7b, there is a nice linear correlation between $\ln(C/C_0)$ and the reaction time ($t$). This experimental fact indicates that the photo decolorization reaction of MO molecules photocatalyzed by the as-obtained products follows the first-order kinetics: [26]

$$-\frac{dC}{dt} = kC$$

wherein C stands for the real-time concentration of the MO molecules, $t$ represents the reaction time, and $k$ stands for the rate constant. The rate constants of the photocatalytic decolorization of MO by the as-obtained porous AgBr/Ag composite microspheres are determined to be 0.105 $min^{-1}$ ($AgNO_3$:CuBr = 0.5:1), 0.135 $min^{-1}$ ($AgNO_3$:CuBr = 1:1), 0.076 $min^{-1}$ ($AgNO_3$:CuBr = 2:1), 0.053 $min^{-1}$ ($AgNO_3$:CuBr = 3:1), respectively, which are distinctly higher than that of the previously P25-$TiO_2$ (0.0065 $min^{-1}$ for MO). The rate constant of the photocatalytic decolorization of MO showed the highest when the ratio of $AgNO_3$ to CuBr was 1:1. Besides the excellent catalytic activity, the recyclability of the catalysts is another principle substantially required by high-quality catalytic species. The durability of the as-obtained porous AgBr/Ag-based plasmonic photocatalysts was also evaluated in terms of performing the MO bleaching reactions repeatedly several times. As shown in Fig. 7d, the catalytic performances in terms of MO decolorization display only trivial decrease under visible-light irradiation after four times. Moreover, the morphology of the as-obtained porous AgBr/Ag nanostructures almost displayed no obvious change after several bleaching tests as shown in Fig. S5. These experimental facts suggest that the as-obtained porous AgBr/Ag microspheres could be employed as stable plasmonic photocatalysts for the bleaching of organic pollutants under visible-light irradiation.

In order to further investigate visible-light catalytic activity of the obtained AgBr/Ag photocatalysts, the colorless phenol was also chosen as a target organic pollutant to evaluate the activity of the as-obtained products. For comparison, P25-$TiO_2$ and N-$TiO_2$ nanoparticles were used as photocatalysts in control experiments, and their UV–vis absorption spectra were provided in Fig. S4, and the N-$TiO_2$ nanoparticles exhibit enhanced absorption in the visible-light region in comparison with P25-$TiO_2$. Besides P25-$TiO_2$ and N-$TiO_2$, the photocatalytic activities of the above as-obtained AgBr/Ag samples were tested and shown in Fig. 8. The photocatalytic results revealed that the AgBr/Ag ($AgNO_3$:CuBr = 1:1) composite microspheres can decompose 79% of 10 mg $L^{-1}$ phenol within 180 min of visible-light irradiation while the P25-$TiO_2$ and N-$TiO_2$ nanoparticles can only decompose 14% and 34% of phenol during the same interval, respectively. In addition, the inset in Fig. 8 shows that the rate constants of the photocatalytic degradation of phenol by the as-obtained porous AgBr/Ag microspheres are estimated to be 0.0067 $min^{-1}$ ($AgNO_3$:CuBr = 0.5:1), 0.086 $min^{-1}$ ($AgNO_3$:CuBr = 1:1), 0.0052 $min^{-1}$ ($AgNO_3$:CuBr = 2:1), 0.0047 $min^{-1}$ ($AgNO_3$:CuBr = 3:1), respectively, which are

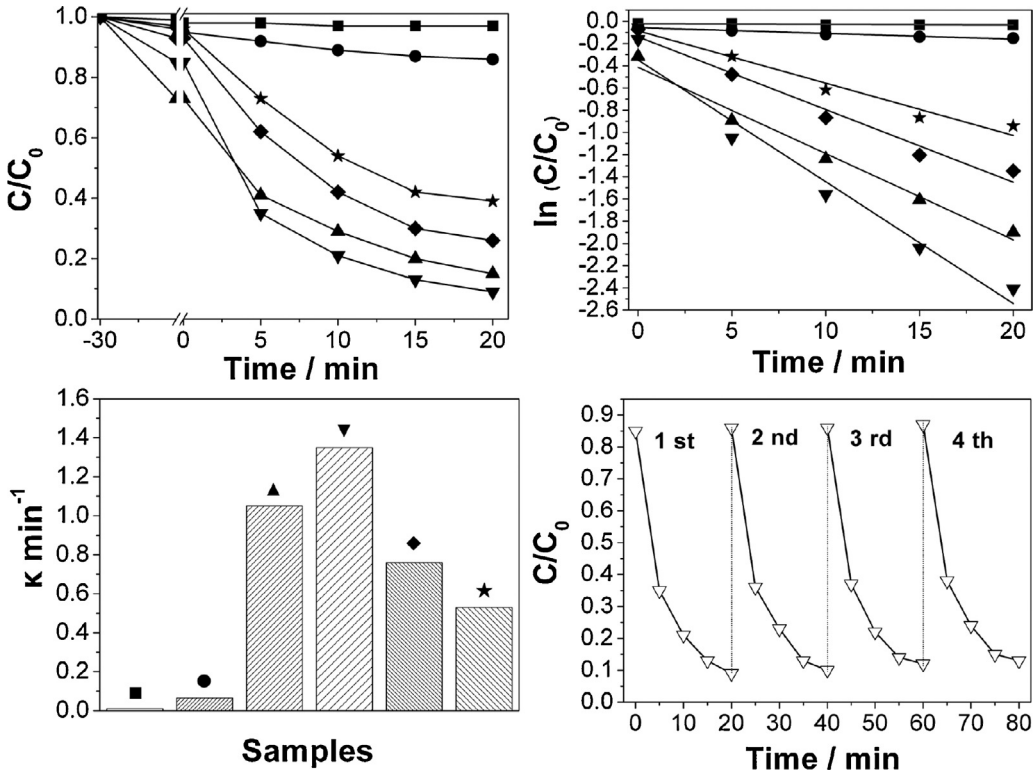


**Fig. 7.** (a) Photodegradation of MO by different photocatalysts under visible-light irradiation (■ a blank experiment, where no catalyst is used, ● commercially available P25-$TiO_2$, and AgBr/Ag composite microspheres synthesized with different ratios of $AgNO_3$ to CuBr (▲ 0.5:1, ▼ 1:1, ♦ 2:1 and ★ 3:1), (b) kinetic linear simulation curves, (c) kinetic constants, and (d) recycling performance of AgBr/Ag (▼ 1:1).

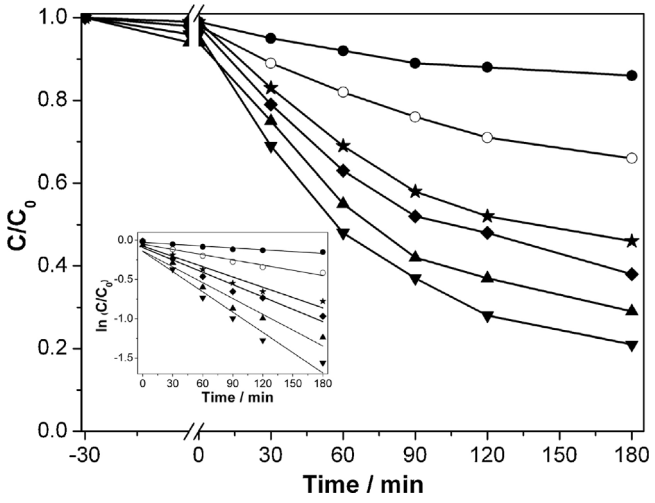


**Fig. 8.** (a) Photodegradation of phenol by different photocatalysts under visible-light irradiation (● commercially available P25-$TiO_2$, ○ N-$TiO_2$, and AgBr/Ag composite microspheres synthesized with different ratios of $AgNO_3$ to CuBr (▲ 0.5:1, ▼ 1:1, ♦ 2:1 and ★ 3:1), the inset shows kinetic linear simulation curves.

distinctly higher than that of P25-$TiO_2$ and N-$TiO_2$ (0.0008 and 0.0022 $min^{-1}$ for phenol). And the highest photocatalytic degradation rate constant of AgBr/Ag (CuBr:$AgNO_3$ = 1:1) was about 10.8 and 3.9 times higher than that of P25-$TiO_2$ and N-$TiO_2$ nanoparticles.

From the above experimental results, the as-obtained products exhibited similar photocatalytic activity both for MO and phenol, and the as-obtained AgBr/Ag microspheres ($AgNO_3$:CuBr = 1:1) showed the highest photocatalytic capability under visible-light illumination among all the obtained products. The reason might be ascribed to two aspects including the content of Ag and specific surface area of the AgBr/Ag composite microspheres in our experiments. The specific surface areas of the as-obtained AgBr/Ag plasmonic photocatalysts showed that their BET surface areas decreased with increasing Ag content, and their values were 0.304, 0.257, 0.036 and 0.006 $m^2 g^{-1}$, respectively. And the experimental results showed that the AgBr/Ag composite microspheres (CuBr:$AgNO_3$ = 1:0.5) exhibited better adsorptive ability for pollutant molecules than all other AgBr/Ag microspheres, and also showed higher photocatalytic performance than other AgBr/Ag composite microspheres (CuBr:$AgNO_3$ = 1:2 and 1:3), which might attribute to that higher specific surface area results in higher adsorption capability and larger contact area for photocatalysis. However, the AgBr/Ag composite microspheres (CuBr:$AgNO_3$ = 1:0.5) with the highest surface area still exhibited lower photocatalytic performance than the AgBr/Ag composite microspheres (CuBr:$AgNO_3$ = 1:1), which may be related to the content of Ag in the AgBr/Ag composite microspheres, since photocatalytic performance was also strongly influenced by the content of Ag in previously reported similar composite catalyst [45,46]. For the as-obtained AgBr/Ag composite microspheres, Ag nanoparticles would produce photogenerated electrons and holes under visible-light illumination, which can be separated by the SPR-induced local electro-magnetic field [11,26,45–47]. However, it was reported that the interface between the AgBr and Ag would be enlarged with the increase of the Ag content, thereby increasing hole capture by the negative surface charge on the Ag nanoparticles, which may reduce the efficiency of charge separation [46]. Furthermore, the increasing content of Ag nanoparticles on the surface of AgBr/Ag composite microspheres blocked the pores seen in Fig. 3, and could decrease the light penetration into the composite microspheres, so the internal reflection enhanced light absorption effect was less prominent. In summary, the proper

content of Ag and specific surface area of AgBr/Ag microspheres in our experiments made the AgBr/Ag microspheres ($CuBr:AgNO_3$ = 1:1) behave the highest catalytic activities.

## 4. Conclusions

A novel and economic sacrificial template method was developed for fast synthesis of porous AgBr/Ag microsphere by using CuBr microsphere as a chemical template. The CuBr template could provide both $Br^-$ ion and $Cu^+$ ion to react with $Ag^+$ ion and generated AgBr and metallic Ag, respectively. The synergistic in-situ reaction mechanism was proposed that the ion-exchange reaction proceeded between CuBr microspheres and $Ag^+$ ions followed by in-situ $Ag^+$ reduction reaction. Furthermore, the photocatalytic performance of porous AgBr/Ag composite microsphere with different composition was investigated through the decolorization of MO and the degradation of phenol under visible-light irradiation, and almost all the MO could be bleached in 20 min while 79% of phenol could be degraded in 180 min by using AgBr/Ag with ratio 1:1, which displayed superior visible-light-driven photocatalytic activity. Additionally, the reported template method and corresponding formation mechanism opens up a new possibility to fabricate other composite materials.

## Acknowledgments

This work was supported by the Natural Science Foundation of China (No. 51102077, No. 51372070 and No. 21203055), the Excellent Youth Scientific Research Foundation of Henan University (0000A40409) and Changjiang Scholars and Innovative Research Team in University (No. PCS IRT1126).

## Appendix A. Supplementary data

Supplementary data associated with this article can be found, in the online version, at http://dx.doi.org/10.1016/j.apcatb.2015.04.027.

## References

[1] D. Ravelli, D. Dondi, M. Fagnoni, A. Albini, Chem. Soc. Rev. 38 (2009) 1999–2011.
[2] M.R. Hoffmann, S.T. Martin, W.Y. Choi, D.W. Bahnemann, Chem. Rev. 95 (1995) 69–96.
[3] X. Chen, S.S. Mao, Chem. Rev. 107 (2007) 2891–2959.
[4] I. Paramasivam, H. Jha, N. Liu, P. Schmuki, Small 8 (2012) 3073–3103.
[5] T.P. Yoon, M.A. Ischay, J. Du, Nat. Chem. 2 (2010) 527–532.
[6] N. Serpone, A.V. Emeline, J. Phys. Chem. Lett. 3 (2012) 673–677.
[7] H. Tong, S. Ouyang, Y. Bi, N. Umezawa, M. Oshikiri, J. Ye, Adv. Mater. 24 (2012) 229–251.
[8] W. Hou, S.B. Cronin, Adv. Funct. Mater. 23 (2012) 1612–1619.
[9] Y. Tian, T. Tatsuma, J. Am. Chem. Soc. 127 (2005) 7632–7637.
[10] M. Long, C. Weimin, Nanoscale 6 (2014) 7730–7742.
[11] C. An, S. Peng, Y. Sun, Adv. Mater. 22 (2010) 2570–2574.
[12] H. Cheng, B. Huang, P. Wang, Z. Wang, Z. Lou, J. Wang, X. Qin, X. Zhang, Y. Dai, Chem. Commun. 47 (2011) 7054–7056.
[13] Q. Dong, Z. Jiao, H. Yu, J. Ye, Y. Bi, Cryst. Eng. Comm. 16 (2014) 8317–8321.
[14] B. Li, H. Wang, B. Zhang, P. Hu, C. Chen, L. Guo, ACS Appl. Mater. Interfaces 5 (2013) 12283–12287.
[15] G. Luo, X. Jiang, M. Li, Q. Shen, L. Zhang, H. Yu, ACS Appl. Mater. Interfaces 5 (2013) 2161–2168.
[16] J. Song, I. Lee, J. Roh, J. Jang, RSC Adv. 4 (2013) 4558–4563.
[17] P. Wang, B. Huang, Z. Lou, X. Zhang, X. Qin, Y. Dai, Z. Zhaoke, Chem.- Eur. J. 16 (2010) 538–544.
[18] W. Wang, H. Du, R. Wang, T. Wen, A. Xu, Nanoscale 5 (2013) 3315–3321.
[19] H. Xu, H. Li, J. Xia, S. Yin, Z. Luo, L. Liu, L. Xu, ACS Appl. Mater. Interfaces 3 (2010) 22–29.
[20] T. Yan, X. Yan, R. Guo, W. Zhang, W. Li, J. You, Catal. Commun. 42 (2013) 30–34.
[21] T. Yan, H. Zhang, Q. Luo, Y. Ma, H. Lin, J. You, Chem. Eng. J. 232 (2013) 564–572.
[22] C.H. Zhang, L.H. Ai, L.L. Li, J. Jiang, J. Alloy. Compd. 582 (2014) 576–582.
[23] M. Zhu, P. Chen, M. Liu, ACS Nano 5 (2011) 4529–4536.
[24] H. Zhang, X. Fan, X. Quan, S. Chen, H. Yu, Environ. Sci. Technol. 45 (2011) 5731–5736.
[25] M. Zhu, P. Chen, M. Liu, J. Mater. Chem. 22 (2012) 21487–21494.
[26] P. Wang, B.B. Huang, X.Y. Qin, X.Y. Zhang, Y. Dai, J.Y. Wei, M.H. Whangbo, Angew. Chem. Int. Ed. 47 (2008) 7931–7933.
[27] L. Kuai, B. Geng, X. Chen, Y. Zhao, Y. Luo, Langmuir 26 (2010) 18723–18727.
[28] B. Ma, J. Guo, W. Dai, K. Fan, Appl. Catal. B: Environ. 130 (2013) 257–263.
[29] Y. Bi, J. Ye, Chem. Commun. (2009) 6551–6553.
[30] W.S. Choi, G.Y. Byun, T.S. Bae, H. Lee, ACS Appl. Mater. Interfaces 5 (2013) 11225–11233.
[31] P. Wang, B. Huang, X. Zhang, X. Qin, H. Jin, Y. Dai, Z. Wang, J. Wei, J. Zhan, S. Wang, J. Wang, M. Whangbo, Chem.- Eur. J. 15 (2009) 1821–1824.
[32] Y. Tang, Z. Dong, Z. Chen, Z. Jiang, G. Xing, A.K.P. Li, Y. Zhang, T.C. Sum, S. Li, X. Chen, Adv. Funct. Mater. 23 (2013) 2932–2940.
[33] X. Xiao, L. Ge, C. Han, Y. Li, Z. Zhao, Y. Xin, S. Fang, L. Wu, P. Qiu, Appl. Catal. B: Environ. 163 (2015) 564–572.
[34] L. Sun, R. Zhang, Y. Wang, W. Chen, ACS Appl. Mater. Interfaces 6 (2014) 14819–14826.
[35] Y. Liu, J. Goebl, Y. Yin, Chem. Soc. Rev. 42 (2013) 2610–2653.
[36] J.N. Gao, Q.S. Li, H.B. Zhao, L.S. Li, C.L. Liu, Q.H. Gong, L.M. Qi, Chem. Mater. 20 (2008) 6263–6269.
[37] A. Zielinska-Jureka, E. Kowalska, J.W. Sobczak, W. Lisowski, B. Ohtani, A. Zaleska, Appl. Catal. B: Environ. 101 (2011) 504–514.
[38] E. Grabowska, J. Reszczynska, A. Zaleska, Water Res. 46 (2012) 5453–5471.
[39] J. Reszczyńska, T. Grzyb, J.W. Sobczak, W. Lisowski, M. Gazda, B. Ohtani, A. Zaleska, Appl. Catal. B: Environ. 163 (2015) 40–49.
[40] J. Choi, H. Park, M.R. Hoffmann, J. Phys. Chem. C 114 (2010) 783–792.
[41] G. Tian, Y. Chen, H.L. Bao, X. Meng, K. Pan, W. Zhou, C. Tian, J.Q. Wang, H. Fu, J. Mater. Chem. 22 (2012) 2081–2088.
[42] Y. Tang, V.P. Subramaniam, T.H. Lau, Y. Lai, D. Gong, P.D. Kanhere, Y.H. Cheng, Z. Chen, Z. Dong, Appl. Catal. B: Environ. 106 (2011) 577–585.
[43] Y. Wang, T. Gao, K. Wang, X. Wu, X. Shi, Y. Liu, S. Lou, S. Zhou, Nanoscale 4 (2012) 7121–7126.
[44] P. Wang, B.B. Huang, X.Y. Zhang, X.Y. Qin, Y. Dai, Z.Y. Wang, Z.Z. Lou, ChemCatChem 3 (2011) 360–364.
[45] M.S. Zhu, P.L. Chen, M.H. Liu, Langmuir 28 (2012) 3385–3390.
[46] J. Jiang, L. Zhang, Chem. Eur. J. 17 (2011) 3710–3717.
[47] B.Z. Tian, T.T. Wang, R.F. Dong, S.Y. Bao, F. Yang, J.L. Zhang, Appl. Catal. B: Environ. 147 (2014) 22–28.